Study of γ-Alumina-Supported Hydrotreating Catalyst: I. Adsorption of Bare MoS_2 Sheets on γ-Alumina Surfaces

Andrei Ionescu, Alain Allouche,* Jean-Pierre Aycard, and Michel Rajzmann

Physique des Interactions Ioniques et Moléculaires, UMR 6633 CNRS & Université de Provence, avenue Escadrille Normandie Niemen, 13397, Marseille Cedex 20 France

Raphael Le Gall

Total S. A., CERT, BP 27, 76700 Harfleur, France

Received: February 10, 2003; In Final Form: May 16, 2003

We herein report on the PW-DFT study of molybdenum disulfide catalyst supported on γ-alumina. An Mo_4S_8 sheet, in a complete periodical environment, was docked to three surfaces of alumina. We found that the alumina surface controlled the orientation and the morphology of MoS_2 sheets. The results show that for all alumina surfaces the Mo-edge- and Mo−S-edge-adsorbed MoS_2 sheets are the most stable configurations.

1. Introduction

Hydrodesulfurization (HDS) is the catalytic process used to produce fuels with greatly reduced levels of sulfur and plays a key role in controlling the S emissions such as SO_x. In the past few years, γ-alumina supported MoS_2 catalysts with Ni or Co as promoter have by far been the most widely used catalytic systems for the HDS reaction.

The catalysts for the HDS reaction are based on sulfides of transition metals (TM) such as sulfided $CoO-MoO_3/\gamma$-Al_2O_3, $NiO-MoO_3/\gamma$-Al_2O_3, and to a much lesser extent $NiO-WO_3/\gamma$-Al_2O_3. Mo is present as a monolayer[1,2] in the form of tetrahedral Mo oxide (low Mo loadings) and octahedral Mo oxide (high Mo loadings). During the sulfiding process, O is replaced by sulfur, thus creating well-organized slabs of molybdenum disulfide, MoS_2.[3]

Even if the mechanism of the HDS reaction has been well clarified, there is a limited fundamental understanding of the actual interaction between the catalyst and the support. The widespread interest in HDS reaction has resulted in a quantity of theoretical papers dealing with fundamental aspects of MoS_2 catalytic action over the past three decades. From empirical methods all the way to ab initio theory, all approaches tended to substitute the lack of experimental information on the chemical properties of catalyst surface and adsorbates. The Huckel tight-binding method[4] and the extended Huckel theory[5] were used to investigate the electronic factors governing thiophene HDS on MoS_2 as well as the nature and activity of the adsorption sites of the catalyst surface. Thiophene interaction with MoS_2 was also studied at the molecular mechanics level.[6] MoS_2 solid was modeled at ab initio level by clusters of several sizes: MoS_6,[7] Mo_3S_9,[8] Mo_2S_{24},[9] Mo_2S_9,[10] and $Mo_2S_{10}H_{12}$.[11]

More recently, density functional calculations were resorted to in studying the structure and active sites of the catalyst. The models used to represent the catalyst ranged from clusters of different sizes to stoichiometric electroneutral single-layer MoS_2 chains.[12] A systematic theoretical study of structure and electronic properties of the clean MoS_2 edge surface was carried out on a $Mo_{24}S_{48}$ periodical unit.[13] An hexagonal geometrical model was developed by ref 14 and further used by other studies.[9,15,16]

Our particular focus is the clarification of MoS_2 nanostructure orientation on γ-Al_2O_3 in order to characterize the interaction between the catalyst and the support. In previous papers we investigated the γ-Al_2O_3 surface reactivity by adsorbing probe molecules such as CO, H_2O, and H_2S on alumina clusters[18] and alumina surfaces by a periodical approach[19] and by a mixed quantum mechanics/molecular mechanics (QM/MM) method.[20] We determined that there was a strong relation between γ-alumina reactivity and the nature of the exposed surface. The (110C) surface was the most reactive, followed by the (110D) surface and the (100) surface.

In this new study, we focused on the adsorption of bare MoS_2 sheets. No promoter was considered. We propose a periodical PW-DFT approach that makes use of crystal periodic boundary conditions and symmetry, and consequently, better describes the two systems and their interaction. Our model was based on the assumption that Mo exists in a pseudomorphic monolayer oxide on γ-Al_2O_3, and that during sulfiding the well-organized MoS_2 sheets fit with the γ-Al_2O_3 unit cell. Thus, Mo appears in the form of ions sandwiched by S atoms in a trigonal prismatic coordination. Our model considered a four-layer sheet of MoS_2 fitted to the γ-Al_2O_3 unit cell, and we investigated the nature of the interaction between the catalyst and the support.

2. Computational Method

In the present work density functional theory calculations employed both the generalized gradient approximation (GGA)[21,22] and the local density approximation (LDA). For the calculations we used the total energy plane wave pseudopotential code, Castep.[23] The cutoff energy varied from 260 to 300 eV. The electron−ion interactions were described using nonlocal reciprocal-space pseudopotentials in the Kleinman-Bylander form.[24] Calculations were done for a Monkhorst Pack grid,[25,26] for the Brillouin zone integration of k points, with 0.1 $Å^{-1}$ spacing.

* Corresponding author. E-mail: Alain.Allouche@piimsdm.univ-mrs.fr.

10.1021/jp0343382 CCC: $25.00
Published on Web 07/10/2003

The MoS_2 sheets adsorption energies on alumina surfaces were calculated as follows:

$$E_{ads} = E_{(MoS_2+Surface)} - E_{(Surface)} - E_{(MoS_2)} \quad (1)$$

where $E_{(MoS_2+Surface)}$ refers to the energy of the system formed by the adsorbed MoS_2 sheet and the surface, $E_{(Surface)}$ refers to the energy of the bare surface, and $E_{(MoS_2)}$ refers to the energy of the isolated MoS_2 sheet in its adsorbed geometry.

All systems were periodic within the supercell approach. The surface of alumina was modeled by two-dimensional periodic slabs of 3−5 layers with a vacuum of 15 Å between slabs in the *x* direction of the crystal, which is perpendicular to the surface plane. An Mo_4S_8 sheet was docked to alumina surfaces in two orientations: perpendicular and parallel to the alumina surfaces.

3. Results and Discussion

3.1. γ-Al_2O_3 Surfaces. γ-Alumina has a spinel-like structure ($MgAl_2O_4$) in which aluminum atoms are substituted for the magnesium atoms. The ideal Wyckoff spinel-type unit cell[29] consists of a cubic closed-packed stacking of 32 oxygen atoms and 24 aluminum atoms that occupy octahedral and tetrahedral sites (16 octahedral and 8 tetrahedral). The stoichiometry of γ-alumina does not fit the spinel-like unit cell. There are $2(^2/_3)$ vacant cation positions per unit cell and the unit cell contains 32 oxygen atoms and $21(^1/_3)$ aluminum atoms in order to satisfy the stoichiometry.[27] There is controversy concerning the exact localization of vacancies.[41] Experimental studies such as X-ray diffraction (XRD),[37] nuclear magnetic resonance (NMR),[38,39] and neutron scattering[40] have shown contradictory results: vacancies are believed to occupy either octahedral or tetrahedral positions. Some studies even consider that there are cations occupying sites which are vacant in the ideal spinel structure.[40] Recent theoretical studies have calculated that, for the bulk, vacancies in the octahedral sites are energetically preferred.[41,28] However, due to the large number of atoms needed in the simulation cell, γ-alumina cannot be easily modeled by first-principles DFT methods within reasonable calculation time.

We generated the γ-alumina ideal spinel unit cell from crystallographic data.[29] No vacancies were initially introduced into the bulk structure,[19] but only afterward, to fulfill surface's stoichiometry. The surface layers of γ-Al_2O_3 are formed by (111) and (110) surfaces.[31] There are four cation arrangements: A and B layers for the (111) surface, and C and D layers for the (110) surface. Peri's model[32] also considered the (100) surface. According to the models for the active surface proposed previously by refs 31 and 32, we considered three surfaces: the (100) and (110) C-layers and the (110) D-layer. Our choice is supported by neutron diffraction studies on γ-alumina,[33] which have indicated that the surface consists only of (110) and (100) planes; no trace of (111) plane has been found. We obtained the surfaces by cleaving the ideal nonstoichiometric bulk. The stoichiometry of each surface depends on the direction of cleaving, the number of layers, and the dimension of the unit cell. Some surfaces are already stoichiometric, and some must contain vacancies in order to become stoichiometric. In the following we refer to perfect surfaces to describe the unaltered surfaces cleaved from ideal, i.e., no vacancy containing, γ-alumina bulk. As shown in Table 1, the (100) and (110D) surfaces are perfect and stoichiometric; as for the (110C) surface, four vacant cation positions must be considered in order to satisfy the γ-alumina stoichiometry.

TABLE 1: Models of Stoichiometric γ-Alumina

model	no. Al	no. O	no. defects
	Bulk		
stoichiometric spinel[29]	21(1/3)	32	2(2/3)
3 unit cells	64	96	8
tolerable approximation[30]	21	32	3
primitive cell[28]	16	24	2
	Surfaces		
(100) 5-layer	16	24	0
(110D) 3-layer	16	24	0
(110C) 3-layer	16	24	4

TABLE 2: Total Energy of the 8 Nonequivalent Configurations before Optimization

	total energy/eV	E_{rel}/kJ·mol^{-1}
O1O2	−5739.7653609	0.00
O1O3	−5739.7462132	1.85
T1O2	−5735.6210263	399.85
T1O3	−5735.6211289	399.84
T1T2	−5732.5523776	695.91
T3T4	−5732.5493276	696.20
T1T3	−5733.9277628	563.21
T1T4	−5733.9948248	556.74

In a previous study[19] we investigated in detail the reconstruction and the reactivity of the (100) and (110D) perfect surfaces. Consequently, in the current study for these two surfaces, we used the results previously obtained.

First, we searched for the minimum energy structure of the defective (110C) surface. The nonprimitive stoichiometric work cell ($a = 17.79$ Å; $b = 15.80$ Å; $c = 5.58$ Å), cleaved from the γ-alumina ideal bulk, consists of 24 O atoms, 16 Al atoms and 4 vacancies. The 4 vacancies can be located in octahedral positions, in tetrahedral positions or in both. The total number of combinations equals 4845. This number was too large to be analyzed, so we considered a work cell whose *b* parameter was reduced by a factor of 2. Thus, the smaller work cell ($a = 17.79$ Å; $b = 7.90$ Å; $c = 5.58$ Å) contains 12 O atoms, 8 Al atoms, and 2 cation vacancies. The two vacancies can be both located in octahedral positions (OO), both in tetrahedral positions (TT), or one in tetrahedral position and one in octahedral position (TO). The total number of such combinations is 45 (15 OO, 6 TT, and 24 TO). We studied eight nonequivalent configurations: two were OO, four were TT, and two were TO. Figure 1a shows the distribution of the vacancies across the (110C) surface. This approach is somehow arbitrary, but it is made necessary by the number of combinations we had to deal with. Nevertheless, we believe that our model provides a good representation of the alumina surface reactivity and is consistent with studies performed on the alumina bulk,[28] which established that the most stable stoichiometric configuration is the one with the vacancies located in octahedral cation positions. We performed single-point total-energy calculations at GGA level using a cutoff of 300 eV. The energies of all eight configurations are listed in Table 2. The lowest energy corresponds to an OO configuration. Between the two OO structures there is an energy difference of only 1.85 kJ·mol^{-1}. We arbitrarily chose the O1O2 configuration as a model for the (110C) stoichiometric surface. The work cell that corresponds to the O1O2 configuration was further enlarged by a factor of 2, with the purpose of obtaining the initial nonprimitive work cell cleaved from the alumina bulk.

Second, we investigated the impact of vacancies on the electronic distribution and consequently on the reactivity of the (110C) surface, and we further analyzed the DOS and layer-resolved PDOS of the perfect and defective surfaces. The DOS of the perfect surface (Figure 2a) shows three peaks in the lower

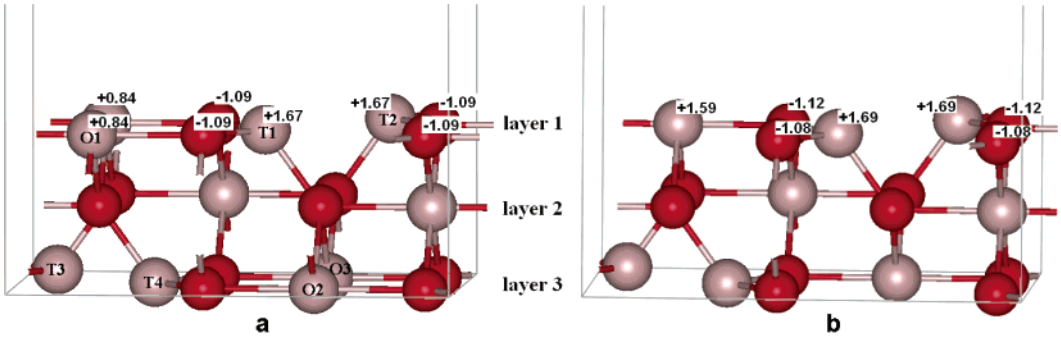

Figure 1. First layer charges for the ideal surface (left) and defective surface (right). Distribution of vacancies on the (110C) surface (left). The selected configurations are (O1O2), (O1O3), (T1T2), (T3T4), (T1T3), (T1T4), (T1O2), and (T1O3).

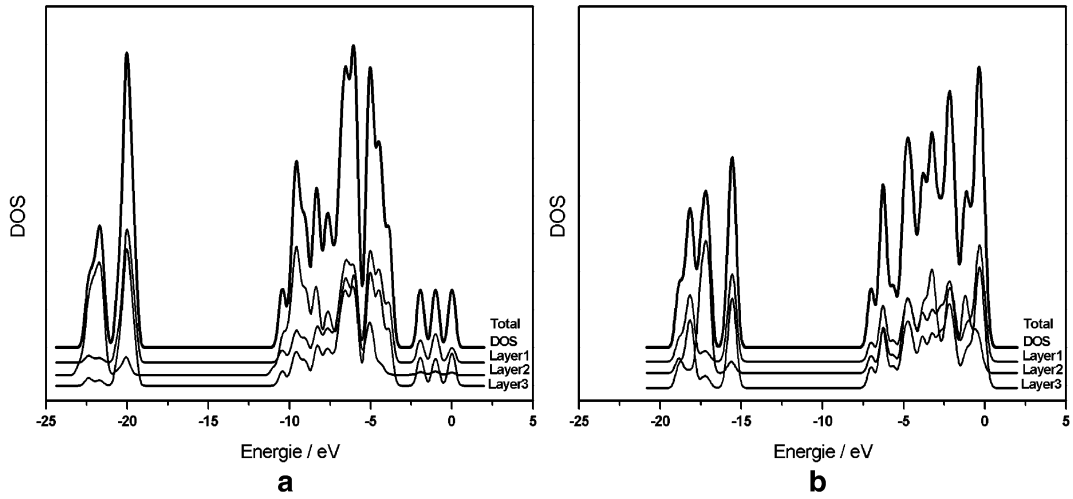

Figure 2. DOS and PDOS of the two systems: (a) ideal surface and (b) defective surface.

valence band (LVB) at −22.3, −21.7, and −20.0 eV. The LVB is mainly formed by the contributions of oxygen atoms. The contribution of aluminum atoms is more important in the upper valence band (UVB). The peak at −22.3 eV is due to the Al atoms of all three layers. The peak at −21.7 eV is due to tricoordinated O atoms of the second layer, and the peak at −20.0 eV is due to the tricoordinated O atoms of the first and third layers. The DOS of the defective (110C) surface (Figure 2b) shows four peaks in the LVB. The peak at −18.7 eV is due to contribution from the Al atoms. The peak at −18.2 eV is due to contributions from tricoordinated O atoms of the first and third layers. The peak at −17.2 eV is due to contributions from O atoms of the second layer. The peak at −15.5 eV is due to contributions from bicoordinated O atoms of the first and third layers. The analysis of the first and third layers PDOS shows that the ideal surface presents one peak due to tricoordinated O atoms and that the defective surface presents two peaks one due to tricoordinated O atoms (at −18.1 eV) and one due to bicoordinated O atoms (at −15.5 eV). The bicoordinated O atoms are located on the first and third layers of the defective surface near the cation vacancies.

The consequences of the vacancies seen on the electronic structure are further supported by a strong electronic density decrease reflected by the atomic net charges (Figure 1) of the vacancy neighboring Al atoms, whose charge varies from +0.84 to +1.59 electrons; for the tetrahedral Al atoms, the charge difference is only 0.02 electron. The charge difference between the tricoordinated O atoms of the defective surface and the bicoordinated ones is 0.04 electron.

We conclude that the introduction of vacancies influenced the reactivity of the (110C) surface. The acid Lewis character of the Al atoms was further accentuated for the defective surface. At the same time, the basic Lewis character of the O atoms was maintained, and the reactivity was altered only at the coordination level; the bicoordinated O atoms are more available than the tricoordinated ones.

Several previous studies investigated in detail the reconstruction of alumina surfaces. It has been shown[35] for the (100) and (110D) surfaces, and our results confirmed[19,20] that there is a small amount of reconstruction, mainly of inner-layer atoms, and the first layer structure is well preserved. As for the (110C) surface, it was previously shown[34] that the three-coordinated Al atoms drop off from the surface layer into vacant octahedral interstices of the next layer, resulting in a situation where only octahedral Al atoms are exposed. Our stoichiometric model for the (110C) surface did not simulate this behavior, as we chose to maintain the three-coordinated Al atoms of the first layer. It is difficult to evaluate the exact impact of this assumption on our results. However, the presence of only octahedral Al atoms on (110C) surface as a result of the optimization conducts to a structure similar to that of the (110D) surface. Moreover, the Al atoms have a small contribution to the interaction between the MoS_2 sheet and alumina surfaces which is mainly of Mo−O type and secondarily of S−Al type. We believe that by not considering the reconstruction of the (110C) surface, we simulated new adsorption sites (tetrahedral Al sites). The periodicity of our approach and the necessity of considering relatively large cells in order to minimize side effects between MoS_2 sheets implied an approach in which all alumina surface layers were completely frozen. Only the MoS_2 sheet was allowed to relax. Consequently, our model refers to the interaction

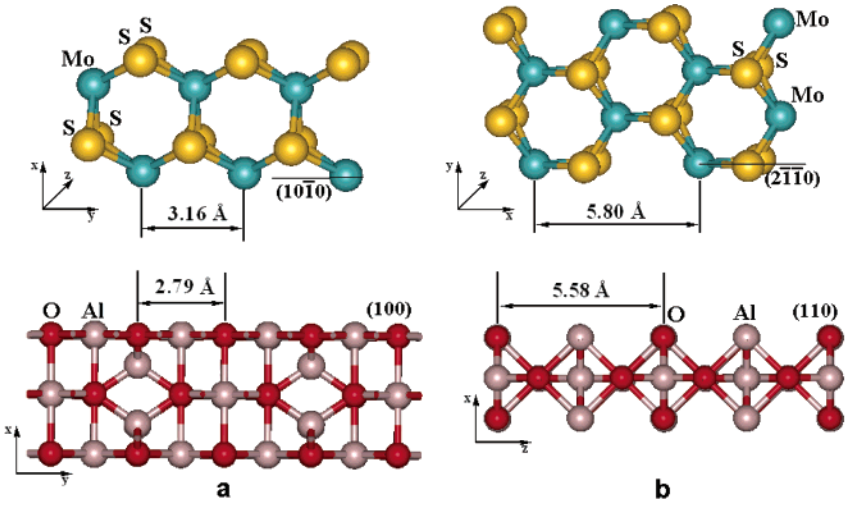

Figure 3. Graphical representation of the models for the MoS_2 sheets and γ-alumina surfaces.

between an MoS_2 sheet and stoichiometric alumina surfaces cleaved from the experimental spinel.

3.2. MoS_2 Sheet. We generated the MoS_2 structure from crystallographic data.[29] Thus, the MoS_2 hexagonal unit cell lattice constants are $a = 3.16$ Å and $b = 12.29$ Å; the space group is $P6_3/mmc$, with two molybdenum atoms occupying the 2c positions with coordinates $\pm(^1/_3,^2/_3,^1/_4)$ and four sulfur atoms occupying the 4f positions with coordinates $\pm(^1/_3,^2/_3,z)$ and $\pm(^1/_3,^2/_3,-z+^1/_2)$ with $z = 0.63$. With these structural parameters the Mo−S distance is 2.42 Å, the angle Mo−S−Mo is 81.6°, and the two angles needed to describe the MoS_6 prism are 81.6° and 135.7° respectively. The distance between two consecutive Mo layers is 6.15 Å and it is 2.98 Å between adjacent S layers. Our model for the MoS_2 is shown in Figure 3. Within each sheet there is a trigonal prismatic unit cell with one central Mo^{4+} cation and six equidistant S^{2-} anions at the corners. We considered three edge-surfaces: (0001) basal plane, (10$\bar{1}$0) Mo edge plane, and (2$\bar{1}\bar{1}$0) Mo−S edge plane. The (0001) basal plane exposes only S atoms in a trigonal prismatic configuration where the S−S distance is 3.16 Å. As previously reported,[44,17] the (0001) basal plane is more stable than the edge planes. This is because the S atoms have three bonds to Mo atoms, whereas the edge planes S atoms have only two bonds to Mo atoms which makes them coordinately unsaturated sites (CUS). Between the (10$\bar{1}$0) and (2$\bar{1}\bar{1}$0) plane, the energy of the latter plane is by 15% higher than that of the former plane.[36,44] The (10$\bar{1}$0) edge plane exposes two types of layers: one layer exposes only unsaturated Mo atoms, and the second layer exposes only unsaturated doubly bridged S atoms.

In our calculation, the molybdenum disulfide sheet was represented by a four-layer, 12-atom slab (Mo_4S_8). Our model of adsorption corresponds to a situation where the MoS_2 unit cell fits the unit cell of alumina surfaces. Consequently, this four-layer 12-atom unit cell was adjusted to fit the experimental unit cell of γ-alumina. As it can be seen on Figure 3, the MoS_2 and Al_2O_3 lattice parameters are very similar, the greatest possible lattice mismatch is 0.37 Å (Figure 3a), while the smallest is 0.22 Å (Figure 3b). Thus the Mo−Mo distance along the y direction is 3.16 Å, by 11.7% greater than the O−O distance along the y direction of the (100) alumina plane. Consequently, we shrank the MoS_2 unit cell by 0.37 Å in order to help it fit with the alumina unit cell. The (2$\bar{1}\bar{1}$0) edge plane exposes only one layer: unsaturated Mo and S atoms at the same time. The Mo−Mo or S−S distance along the x direction is 5.80 Å, greater by 3.9 Å than the O−O or Al−Al distance along the z direction of the (110) alumina plane. This means that in the latter case we shrank the MoS_2 unit cell by 0.22 Å in order to fit it with the alumina unit cell.

Our approach is based on the assumption that in the physical reality the growing crystal adapts its parameters to those of the surface resulting in a pseudomorphic structure of the first layers. The impact of the MoS_2 unit cell fit is minimized by the fact that MoS_2 was allowed to fully relax in two directions while only the third direction was frozen in order to maintain the periodic boundaries of the system. Experimentally it was shown that Mo exists as a monolayer of MoO.[1,2] The support dictates the monolayer oxidic structure and consequently influences the structure of the well-organized MoS_2 sheets obtained after sulfiding. However, we believe that the layers far from the alumina surface tend to regain the experimental MoS_2 structure.

3.3. Adsorption of MoS_2 on γ-Al_2O_3. Our goal was to find the most stable orientation of MoS_2 on the surface of γ-Al_2O_3 and the influence of the support's surface on the nanostructure of the MoS_2 catalyst.

Many models propose for the catalyst structure that the MoS_2 sheet be bonded to alumina through an Mo−O interaction.[42−44] However, we also considered a bonding model between the MoS_2 sheet and the alumina surfaces based on an S−Al interaction. Following the above bonding schemes we adsorbed a four-layer MoS_2 sheet in three orientations: two were perpendiculars (Mo−O interaction), and one was parallel (S−Al interaction) to alumina surfaces. On the (100) and (110) alumina surfaces, we adsorbed an MoS_2 sheet by (10$\bar{1}$0) Mo edge plane and by (2$\bar{1}\bar{1}$0) Mo−S edge plane. The above configurations correspond to a perpendicular orientation of the MoS_2 sheet on the alumina surfaces. On the (100) and (110) alumina surfaces, we also adsorbed an MoS_2 sheet by (0001) basal plane which corresponds to a parallel orientation. The parallel sheet was obtained by rotating by 90° the perpendicular sheet adsorbed by the (10$\bar{1}$0) Mo edge.

The next two paragraphs present the results, extended geometrical parameters for each model as well as calculated adsorption energies. The last section contains the discussion and the conclusions.

3.3.1. Adsorption on (100) Alumina Surface. Figure 4a shows the equilibrium geometry of perpendicular sheet adsorbed by the (10$\bar{1}$0) Mo edge on the (100) γ-Al_2O_3 surface. The distance between adsorbed Mo atoms of MoS_2 sheet and O atoms of the surface is 2.21 Å. The adsorption energy calculated from eq 1 is −854 kJ·mol^{-1}. The MoS_2 sheet maintains the initial

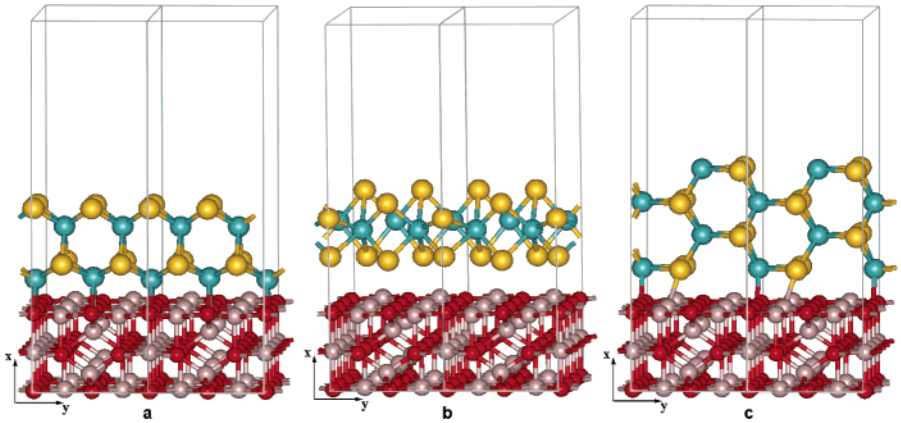

Figure 4. Equilibrium geometries for the adsorption of MoS_2 on γ-alumina (100) plane: (a) perpendicular Mo edge, (b) parallel basal plane, and (c) perpendicular Mo−S edge.

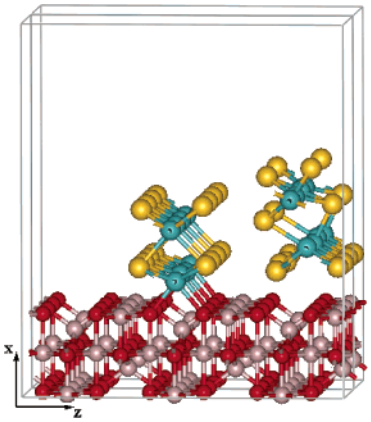

Figure 5. Equilibrium geometries for the adsorption of two MoS_2 sheets on γ-alumina (100) plane.

geometry, and there is interaction between the Mo edge atoms and the O atoms of the surface; each Mo atom interacts by covalent bonding with two O atoms, and the MoS_2 sheet is situated in the middle of the channel formed by two successive O atom rows of the surface.

Figure 4b shows the equilibrium geometry of a parallel sheet adsorbed by the (0001) base plane on the (100) γ-Al_2O_3 surface. The distance between the adsorbed S edge, and the surface is 2.86 Å, which suggests the existence of a weak van der Waals type interaction between the parallel sheet and alumina surface. This is supported by the adsorption energy of -416 kJ·mol^{-1}, twice less important than in the case of a perpendicular sheet.

Figure 4c shows the equilibrium geometry of a perpendicular sheet adsorbed by the $(2\bar{1}10)$ Mo−S edge on the (100) γ-Al_2O_3 surface. The distance between bonded edge Mo atoms and O atoms of the surface is 2.07 Å. The distance between bonded edge S atoms and Al atoms of the surface is 2.06 Å. The adsorption energy is -522 kJ·mol^{-1}.

For the (100) surface in addition to above models we studied the interaction between two MoS_2 sheets and the surface. This was possible because of the relatively large alumina unit cell used to simulate the (100) surface. The sheets were adsorbed in a sandwich configuration and the initial distance between the two sulfur rows of each sheet was about 3.00 Å, i.e., similar to the experimental geometry of MoS_2. One sheet was adsorbed on the Mo edge and one on the S edge. Figure 5 shows the equilibrium geometry. One can see that the sheet adsorbed by the metallic edge interacts with the alumina surface; the distance between the Mo atoms and the O atoms is 2.15 Å, close to the distance of a single perpendicular sheet. As for the S-edge-adsorbed sheet, the interaction is weak, and the distance between S atoms and the alumina surface is 2.47 Å, close to the distance between the parallel sheet and the surface. No energy of adsorption was calculated because of the difficulty to assign interaction contributions between each sheet and the surface.

3.3.2. Adsorption on (110) Alumina C and D layers. There were two layers for the (110) alumina surface: C and D layers. Consequently, in the following, the results refer to adsorption on two different surfaces.

Figure 6a shows the equilibrium geometry of perpendicular sheet adsorbed by the (10 <fraction>*line*10) Mo edge on the (110C) γ-Al_2O_3 surface. The Mo atoms interact with the O atoms of the surface; the Mo−O distance is 2.12 Å. The adsorption energy is -549 kJ·mol^{-1}. The interaction is between a surface Mo atom and a tricoordinated O atom of the surface. The adsorption energy is by 111 kJ·mol^{-1} bigger than that obtained on the tricoordinated atoms of the (110D) surface.

Figure 6b shows the equilibrium geometry of a parallel sheet adsorbed by the (0001) base plane on the (110C) γ-Al_2O_3 surface. The unsaturated S atoms are situated at a distance of 1.94 Å from the surface, and the bridged S atoms are situated at a distance of 2.05 Å. The unsaturated S atoms are bonded to Al atoms by 2.41 Å. The adsorption energy is -346 kJ·mol^{-1} and is consistent with the weak adsorption energies obtained for the parallel sheets.

Figure 6c shows the equilibrium geometry of a perpendicular sheet adsorbed by the $(2\bar{1}10)$ Mo−S edge on the (110C) γ-Al_2O_3 surface. The Mo atoms interact with the O atoms of the surface; the distance is 1.91 Å and corresponds to a strong bonded interaction. The adsorption energy is -592 kJ·mol^{-1}.

Our preliminary investigations[19] showed that for the (110D) surface there are two sites of adsorption corresponding to two types of O atoms exposed: bicoordinated O atoms and tricoordinated O atoms. Our calculations showed that the adsorption on bicoordinated O atoms was more stable that the adsorption on tricoordinated O atoms. Consequently, only the results for the bicoordinated O atoms are shown.

Figure 7a shows the equilibrium geometry of perpendicular sheet adsorbed by the $(10\bar{1}0)$ Mo edge on the (110D) γ-Al_2O_3 surface. The distance between the Mo atoms and the O atoms is 1.97 Å and corresponds to a strong interaction between the MoS_2 and the alumina surface. The adsorption energy is -605 kJ·mol^{-1}.

Figure 7b shows the equilibrium geometry of a parallel sheet adsorbed by the (0001) base plane on the (110D) γ-Al_2O_3 surface. Like in the previous cases, the parallel sheet only slightly interacts with the alumina surface. The distance between

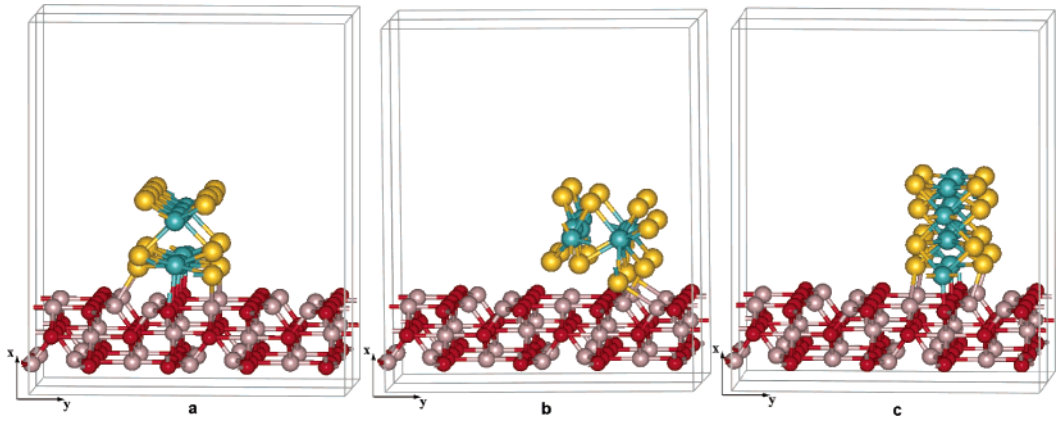

Figure 6. Equilibrium geometries for the adsorption of MoS_2 on γ-alumina (110C) plane: (a) perpendicular Mo edge, (b) parallel basal plane, and (c) perpendicular Mo−S edge.

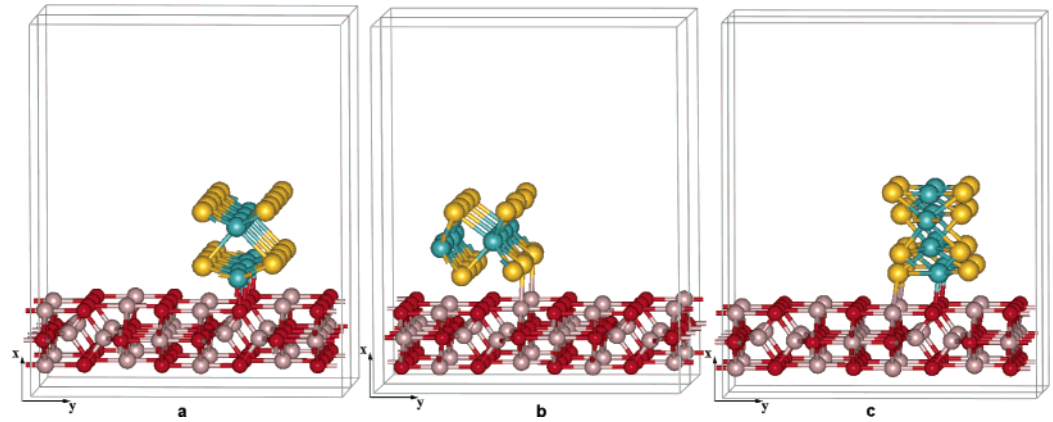

Figure 7. Equilibrium geometries for the adsorption of MoS_2 on γ-alumina (110D) plane: (a) perpendicular Mo edge, (b) parallel basal plane, and (c) perpendicular Mo−S edge.

the S edge and the alumina surface is 2.34 Å in the case of the unsaturated S atoms and 1.87 Å in the case of the bridged S atoms. The adsorption energy is −255 kJ·mol^{-1}.

Figure 7c shows the equilibrium geometry of a perpendicular sheet adsorbed by the $(2\bar{1}10)$ Mo−S edge on the (110D) γ-Al_2O_3 surface. The distance between the Mo atoms and the O atoms of the surface is 1.92 Å. The adsorption energy is −524 kJ·mol^{-1}.

On all surfaces we found that the MoS_2 sheet was preferentially adsorbed in a perpendicular orientation. For all perpendicular orientations, the interaction between the catalyst and the support produces strong covalent bonds whereas for the parallel orientation the equilibrium geometries suggest that the interaction is essentially of the van der Waals type.

4. Discussion and Conclusion

We believe that in the study of heterogeneous catalysts one must consider the influence of the entire surface as well as the bulk environment in order to efficiently characterize the geometry and chemistry of the active sites. In this work we resorted to PW-DFT calculations to study the interaction between a four-layer adjusted MoS_2 sheet and γ-alumina in a complete periodical environment. Our model rests on the assumption that, given the similarity between the MoS_2 Mo−Mo or S−S distance intra- and interslab and the O−O or Al−Al distance in Al_2O_3, the catalyst fits the support. A better approach could have been the adsorption of MoS_2 clusters on alumina surfaces, but if side effects are to be minimized, this requires large simulation cells and therefore indefinite simulation times. We believe that our model is the best alternative to cluster models.

Experimentally there is some controversy concerning the orientation of MoS_2 sheets on alumina. It was shown that with the rise of the sulfiding temperature, the interaction between MoS_2 and Al_2O_3 decreases, which, at high sulfiding temperatures, leads to a point where the MoS_2 crystallites are stabilized by weak van der Waals forces, between the basal plane and the alumina surface, in a parallel orientation.

It was also shown that there is a strong interaction between molybdenum oxides (MoO_x) and the γ-Al_2O_3 support, which produces a highly dispersed monolayer of MoO_x before sulfidation.[2] The structure of MoO_x oxides dictates on the structure of highly ordered MoS_2 sheets. It was also shown[31] that the different surface structures of γ-Al_2O_3 leads to different natures of hydroxyl groups on each surface plane. Consequently we believe that the surface structure of γ-Al_2O_3 has a major role and influence on the nanostructure of MoS_2 sheets.

Experimentally, the effects of surface orientation and crystallinity of γ-Al_2O_3 on the nanostructure of MoS_2 clusters were investigated by the means of X-ray photoelectron spectroscopy (XPS) and transmission electron microscopy (TEM).[42,43] The results showed that on the (100) alumina surface the MoS_2 clusters were edge-bonded in a perpendicular orientation, while on the (110) alumina surface the MoS_2 clusters were basal-bonded in a parallel orientation. In both cases the presence of interfacial Mo atoms that maintain the arrangement in the oxide states is believed to account for the importance of the surface exposed by the support on the orientation of MoS_2 sheets.

TABLE 3: Calculated Adsorption Energies for the MoS_2 Sheet on Alumina Surface

MoS_2 sheet	orientation	Al_2O_3 surface	E_{ads}/kJ·mol^{-1}
$(10\bar{1}0)$	⊥	(100)	−854
		(110C)	−549
		(110D)	−605
(0001)	∥	(100)	−416
		(110C)	−346
		(110D)	−255
$(\bar{2}110)$	⊥	(100)	−522
		(110C)	−592
		(110D)	−524

Theoretically, results obtained on a $Mo_{12}S_{24}$ cluster docked to a limited model of γ-Al_2O_3 by a DFT approach showed that the MoS_2 sheet preferred a perpendicular or near-to-perpendicular orientation to the alumina surface.[9]

Our calculations demonstrated that the perpendicular MoS_2 sheets are bonded to alumina surfaces while the parallel one interacts only slightly. This is because the basal sulfur atoms have completely filled $3s^23p^6$ octets, while the edge sulfur atoms are coordinately unsaturated, which makes them more reactive. We believe that the difference in reactivity between the two orientations of MoS_2 sheets and alumina surfaces influences the catalytic activity. Moreover, the MoS_2 morphology itself has a major role in the catalytic activity as corner and edge plane sites along MoS_2 edges are believed to have different catalytic activities.

Our calculations showed that on all alumina surface planes, the MoS_2 perpendicular sheet was the most stable orientation. However, we cannot clearly distinguish the most reactive alumina surface and the most stable structure between Mo edge and Mo−S edge because the calculated adsorption energies are of the same order with only one exception: the adsorption energy of the perpendicular MoS_2 sheet by $(10\bar{1}0)$ Mo edge plane on the (100) alumina surface (Table 3). The relatively large energy difference is explained by the interaction between Mo atoms and two ranges of O atoms of the surface, whereas in all the other cases the interaction is between Mo atoms and a single range of O surface atoms. For the parallel adsorbed MoS_2 sheet, the stability increases in the order of (100D) > (110C) > (100); the most stable parallel sheet was found on the (100) surface because of the arrangement of octahedral Al atoms which favored the adsorption by the sulfur edge plane. Due to periodic constraints we were unable to study a parallel monolayer of MoS_2 on the (110) surface as predicted by experimental studies.[43]

The most interesting result is obtained in the case of consecutive adsorption of two MoS_2 sheets on (100) alumina surface (Figure 5). The Mo edge interacts with the surface by covalent bonding between Mo and O atoms, while The S edge interacts slightly; i.e., no bonding is observed between the S atoms and the Al atoms of the surface. However, the distance between the S atoms and the alumina surface is 2.47 Å, suggesting a stronger interaction than that observed between the basal plane of the parallel sheet and the alumina surface. This indicates that the S-edge-adsorbed sheet is stabilized by lateral interactions with the Mo-edge-adsorbed sheet. The mean distance between the two S rows of the MoS_2 sheets is 3.38 Å, which is close to the experimental distance (2.98 Å) between MoS_2 crystal layers.

The consecutive adsorption was important because it gave us the proof of the stability of the perpendicular orientation i.e., adsorption by Mo edge and Mo−S edge. Considering the most stable orientations we suppose that the well-organized MoS_2 phase is stacks of Mo edge or Mo−S edge adsorbed sheets and the distance between alternate surface-bonded sheets is 7.40 Å for the (100) surface, 4.90 Å for the (110D) surface, and 4.60 Å for the (110C) surface. The intersheet distances are related to the distribution of O rows in the support surface. Thus, for the (100) surface it is possible, considering the large lateral distance, that between two surface-bonded MoS_2 sheets an S-edge-adsorbed sheet is present resulting in a situation which generates the MoS_2 crystal structure. As for the (110) surfaces, the lateral distance between MoS_2 sheets is rather close to the experimental distance of 2.98 Å, and no presence of S-edge-adsorbed sheet is possible. In conclusion, considering the above predictions, the most reactive possible configuration is on the (110) surfaces because of the presence of only Mo edge and Mo−S edge surface-bonded sheets.

The approach we propose will be further used to investigate the influence of the promoter, Co or Ni, on the adsorption energies and the orientation of MoS_2 sheets on alumina surfaces.

Acknowledgment. We would like to acknowledge the Total S.A. company for their support. The computations were done at the "Centre Régional de Compétence en Modélisation Moléculaire de Marseille".

References and Notes

(1) Lipsch, J. M. J. G.; Schuit, G. C. A. *J. Catal.* **1969**, *15*, 179.
(2) Topsøe, H.; Clausen, B. S.; Massoth, F. E. *Hydrotreating Catalysis: Science and Technlogy*; Springer-Verlag: Berlin, 1996.
(3) Topsøe, N. *J. Catal.* **1980**, *64*, 235−237.
(4) Zonnevylle, M. C.; Hoffmann, R. *Surf. Sci.* **1988**, *199*, 320.
(5) Jubert, A. H.; Pis-Diez, R.; Estiu, L. Guillermina; Ruette, F. *J. Mol. Struct. (THEOCHEM)* **1999**, *465*, 111.
(6) Brunier, T. M.; Drew, M. G. B.; Mitchell, P. C. H. *J. Chem. Soc. (Faraday Trans.)* **1992**, *88*, 3225.
(7) El Beqqali, O.; Zorkani, I.; Rogemond, F.; Chermette, H.; Chaabane, R. B.; Gamoudi, M.; Guillaud, G. *Synth. Met.* **1997**, *90*, 165.
(8) Mitchell, P. C. H.; Plant, C. *Bull. Soc. Chim. Belg.* **1995**, *104*, 293.
(9) Faye, P.; Payen, E.; Bougeard, D. *J. Catal.* **1998**, *179*, 560.
(10) Harris, S.; Chianelli, R. R. *J. Catal.* **1986**, *98*, 17.
(11) Zakharov, I.; Startsev, A. N.; Zhidomirov, G. M. *J. Mol. Catal.* **1997**, *A119*, 437.
(12) Byskov, L. S.; Norskov, J. K.; Clausen, B. S.; Topsøe, H. *J. Catal.* **1999**, *187*, 109.
(13) Raybaud, P.; Hafner, J.; Kresse, G.; Toulhoat, H. *Surf. Sci.* **1998**, *407*, 237.
(14) Payen, E.; Hubaut, R.; Kasztelan, S.; Poulet, O.; Grimblot, J. *J. Catal.* **1994**, *147*, 123.
(15) Cristol, S.; Paul, J.; Payen, E.; Bougeard, D.; Clémendot, S.; Hutschka, F. *J. Phys. Chem. B* **2000**, *104*, 11220.
(16) Cristol, S.; Paul, J.; Payen, E.; Bougeard, D.; Clémendot, S.; Hutschka, F. *J. Phys. Chem. B* **2002**, *106*, 5659.
(17) Travert, A.; Nakamura, H.; van Santen, R. A.; Cristol, S.; Paul, J.; Payen, E. *J. Am. Chem. Soc.* **2002**, *124*, 7084.
(18) Maresca, O.; Allouche, A.; Aycard, J. P.; Rajzmann, M.; Clémendot, S.; Hutschka, F. *J. Mol. Struct. (THEOCHEM)* **2000**, *505*, 81.
(19) Ionescu, A.; Allouche, A.; Aycard, J.-P.; Rajzmann, M.; Hutschka, F. *J. Phys. Chem. B* **2002**, *106*, 9359.
(20) Maresca, O.; Ionescu, A.; Allouche, A.; Aycard, J. P.; Rajzmann, M.; Clemendot, S.; Hutschka, F. *J. Mol. Struct. (THEOCHEM)* **2003**, *620*, 119.
(21) Perdew, J. P.; Wang, Y. *Phys. Rev. B* **1092**, *46*, 6671.
(22) White, J. A.; Bird, D. M. *Phys. Rev. B* **1994**, *50*, 4954.
(23) Milman, V.; Winkler, B.; White, J.; Pickard, C.; Payne, M.; Akhmatskaya, E.; Nobes, R. *Int. J. Quantum Chem.* **2000**, *77*, 895.
(24) Kleinman, L.; Bylander, D. M. *Phys. Rev. Lett.* **1982**, *48*, 1425.
(25) Monkhorst, H.; Pack, J. *Phys. Rev. B* **1976**, *13*, 5188.
(26) Monkhorst, H.; Pack, J. *Phys. Rev. B* **1977**, *16*, 1748.
(27) Lippens, B. C.; Steggerda, J. J. In *Physical and Chemical Aspects of Adsorbents and Catalysts*; Linsen, B. G., Ed.; Academic Press: London, 1970.
(28) Gutiérrez, G.; Taga, A.; Johansson, B. *Phys. Rev. B* **2002**, *65*, 12101.
(29) Wyckoff, R. W. G. *Crystal Structures*; Interscience Publishers: New York, 1968.

(30) Mo, S. D.; Xu, Y. N.; Ching, W. Y *J. Am. Ceram. Soc.* **1997**, *80*, 1193.
(31) Knözinger, H.; Ratnasamy, P. *Catal. Rev. Sci. Eng.* **1978**, *17* (1), 31.
(32) Peri, J. B. *J. Phys. Chem.* **1965**, *69*, 220.
(33) Beaufils, J.; Barbaux, Y. *J. Chem. Phys.* **1981**, *78*, 347.
(34) Sohlberg, K.; Pennycook, S. J.; Pantelides, S. T. *J. Am. Chem. Soc.* **1999**, *121*, 10999.
(35) Blonski, S.; Garofalini, S. H. *Surf. Sci.* **1993**, *295*, 263.
(36) Hayden, T. F. Ph.D. Thesis, University of Wisconsin-Madison, 1986.
(37) Wang, J. A.; Bokhimi, X.; Morales, A.; Novaro, O.; Lopez, T.; Gomez, R. *J. Phys. Chem.* **1999**, *B103*, 299.
(38) John, C. S.; Alma, N. C. M.; Hays, G. R. *Appl. Catal.* **1983**, *6*, 341.
(39) Lee, M.-H.; Cheng, C.-F.; Heine, V.; Klinowski, J. *Chem. Phys. Lett.* **1997**, *265*, 673.
(40) Zhou, R.-H.; Snyder, R. L. *Acta Crystallogr.* **1991**, *B47*, 617.
(41) Wolverton, C.; Hass, K. C. *Phys. Rev. B* **2000**, *63*, 24102.
(42) Sakashita, Y.; Araki, Y.; Honna, K. *Appl. Catal.* **2000**, *A197*, 247.
(43) Sakashita, Y. *Surf. Sci.* **2001**, *489*, 45.
(44) Hayden, T. F.; Dumesic, J. A. *J. Catal.* **1987**, *103*, 366.